Axon Kinematics Change During Growth and Development

Hailing Hao

David I. Shreiber
e-mail: shreiber@rci.rutgers.edu

Department of Biomedical Engineering,
Rutgers, The State University of New Jersey,
617 Bowser Road,
Piscataway, NJ 08854

*The microkinematic response of axons to mechanical stretch was examined in the developing chick embryo spinal cord during a period of rapid growth and myelination. Spinal cords were isolated at different days of embryonic (E) development post-fertilization (E12, E14, E16, and E18) and stretched 0%, 5%, 10%, 15%, and 20%, respectively. During this period, the spinal cord grew ~55% in length, and white matter tracts were myelinated significantly. The spinal cords were fixed with paraformaldehyde at the stretched length, sectioned, stained immunohistochemically for neurofilament proteins, and imaged with epifluorescence microscopy. Axons in unstretched spinal cords were undulated, or tortuous, to varying degrees, and appeared to straighten with stretch. The degree of tortuosity (ratio of the segment's pathlength to its end-to-end length) was quantified in each spinal cord by tracing several hundred randomly selected axons. The change in tortuosity distributions with stretch indicated that axons switched from non-affine, uncoupled behavior at low stretch levels to affine, coupled behavior at high stretch levels, which was consistent with previous reports of axon behavior in the adult guinea pig optic nerve (Bain, Shreiber, and Meaney, J. Biomech. Eng., **125**(6), pp. 798–804). A mathematical model previously proposed by Bain et al. was applied to quantify the transition in kinematic behavior. The results indicated that significant percentages of axons demonstrated purely non-affine behavior at each stage, but that this percentage decreased from 64% at E12 to 30% at E18. The decrease correlated negatively to increases in both length and myelination with development, but the change in axon kinematics could not be explained by stretch applied during physical growth of the spinal cord. The relationship between tissue-level and axonal-level deformation changes with development, which can have important implications in the response to physiological forces experienced during growth and trauma.* [DOI: 10.1115/1.2746372]

Introduction

Injury to axons in the white matter of central nervous system (CNS) tissue is the largest contributor to physiological and functional deficits following brain and spinal cord trauma [1,2]. Myelinated axons, myelinating glia, and astrocytes are the primary structural constituents in white matter that provide the tissue with mechanical integrity to prevent deformation during trauma. Numerous studies have implicated mechanical strain as the proximal cause of traumatic axonal injury, while secondary ischaemic and excitotoxic insults associated with the primary trauma potentially exacerbate the structural and functional damage [3,4]. During trauma to white matter, macroscopic loading conditions are transferred to the microscopic, cellular components. In many white matter tracts, such as the white matter in the spinal cord, axons are aligned predominantly along the length of tract. If the axons were perfectly straight and completely coupled to the bulk tissue, then, as the spinal cord deformed during trauma, all axons would demonstrate signs of injury at roughly the same level of macroscopic deformation (within the biological variability of the strain thresholds for injury to individual axons). However, several studies have demonstrated that the number of axons demonstrating immunohistopathological, electrophysiological, and functional deficits consistent with mechanical injury, as well as injury to glia surrounding the axonal network, increases with the level of macroscopic stretch [5–10]. These trends are not explained by an increased susceptibility to injury of small caliber axons, which would be consistent with stress-based mechanical failure theories. Though different cytoskeletal changes have been observed in small- versus large-caliber axons exposed to dynamic stretch, no correlation has been observed between "injury" and axon diameter in these models [11–13]. In some instances, larger diameter axons are more likely injured [14,15].

Breig first documented that axons in the spinal cord are not, in fact, perfectly straight, but rather demonstrate pronounced undulation, or tortuosity [16]. A more recent study by Bain et al. showed that axons in the guinea pig optic nerve are also undulated to varying degrees [17]. When excised optic nerves were exposed to controlled levels of stretch, the axons became progressively straighter. The unfolding of the axons did not, however, follow idealized descriptions of neither affine, fully coupled nor non-affine, completely uncoupled mechanical behavior. Instead, axons first appeared to deform independently of each other, and then gradually transitioned to coupled, affine behavior as the magnitude of macroscopic stretch increased. The observed variations in mechanical behavior would cause different axons to reach a single injury threshold value of microscopic axon strain at different magnitudes of macroscopic tissue strain, and would provide a potential explanation for the non-uniform pattern of axonal pathology with increasing injury severity. A tortuous axon that deforms purely in a non-affine manner will not experience stretch—and, therefore, injury—until it has completely straightened, which would significantly decrease the actual axon strain-to-injury threshold from the tissue-level threshold. For instance, parallel studies by Bain estimated the tissue-level strain threshold for morphological injury to guinea pig optic nerve axons to be 21% [9]. If the tortuosity of the axons is taken into consideration, and purely non-affine behavior is assumed, the axon-level threshold drops to 8% strain, based on the mean tortuosity of unstretched axons. The "switch" from non-affine to affine kinematics implies that the actual axon-level threshold lies between the non-affine prediction and the tissue-level prediction. Thus, to include microstructural

Contributed by the Bioengineering Division of ASME for publication in the JOURNAL OF BIOMECHANICAL ENGINEERING. Manuscript received March 28, 2006; final manuscript received February 14, 2007. Review conducted by Cheng Dong.

 Copyright © 2007 by ASME

Downloaded From: https://biomechanical.asmedigitalcollection.asme.org on 04/23/2019 Terms of Use: http://www.asme.org/about-asme/terms-of-use

information in a model of white matter injury mechanics [18], both the tortuosity and the dynamics of axon coupling must be known.

It was hypothesized that the "glial matrix," and, more specifically, oligodendrocytes, which can myelinate over twenty different axonal segments, act to mechanically couple axons during stretch, and thereby inhibit purely non-affine deformation [17]. Additional interactions between axons and oligodendrocytes occur at paranodal junctions, where the axonal cytoskeleton is anchored to the oligodendrocyte through interactions of Caspr and contactin (on the axon side) with neurofascin 155 (on the oligodendrocyte side) [19,20]. Astrocytes, too, may contribute to mechanical coupling via separate contacts with blood vessels in formation of the blood-brain barrier, and with axons at nodes of Ranvier through the call adhesion molecule Necl-1 [21,22]. Axon coupling via the glial matrix has clear importance for axonal injury mechanics, and also has strong implications for injury to glia. For example, just as axonal pathology increases progressively with higher levels of applied stretch, so does injury to glia. It is known that oligodendrocyte death is an important component in the progression of white matter injury that further limits axon regeneration and remyelination [23,24], yet only recently has the primary injury response of these cells from mechanical trauma been investigated [24].

Many changes occur during development that may influence axon tortuosity and coupling. For instance, in the human, myelination of the spinal cord is incomplete at birth and continues until at least 3 years of age [25], and maturation of white matter fiber tracts (thickening of axons and myelin sheaths) can continue well into adolescence, especially in tracts involved in motor pathways [26]. Additionally, during this time the spinal cord lengthens significantly from the physical forces experienced during growth, which may also affect axon morphology.

To begin to examine the influence of these changes on axon kinematics, we characterized the kinematic response of axons following in situ stretch of the chick embryo spinal cord during a period of rapid myelination and growth (>50% increase in length in the segment of spinal cord examined). Although the chick CNS begins developing ~21 h post-fertilization [27], and functional axons are present at E7 (embryonic day 7, i.e., 7 days post-fertilization) [28], maturation of the oligodendrocyte phenotype and subsequent myelination of axons does not begin until several days later. For instance, the myelination process begins in the ventral funiculus of the chick spinal cord at E10, with the first compact myelin observed at E12 [29]. The process follows a sigmoidal curve, slowly increasing until E14, where it enters the linear portion of the sigmoid. At hatching (E21), 60% of axons in the ventral funiculus are myelinated. Myelination of other regions of the spinal cord can follow slightly different time courses, but generally begins prior to myelination in the cerebral cortex [30]. As the degree of myelination increases, the level of coupling of axons to the glial matrix should also increase. During this time, the spinal cord is increasingly vascularized, which may also increase mechanical coupling via astrocytes. Thus, we expect axons to demonstrate increasingly affine—or mechanically coupled—behavior as development and myelination progress.

Methods

Chick Embryo Spinal Cord Measurement and Isolation. Fresh fertile chicken eggs (Charles River Laboratories, Wilmington, MA) were incubated to one of four developmental stages (E12, E14, E16, or E18), and the full spinal column with spinal cord intact was excised. The ventral surface of the spinal cord was exposed. The gauge length of a segment of the spinal cord beginning at the first nerve root after the cervical enlargement and extending rostrally for 11 segments was measured. Each measurement was repeated three times for the average value. After the final measurement, the dorsal half of the vertebrate was removed to allow free stretch of the spinal cord, and the length of spinal cord was re-measured. Each measurement was again repeated three times after full dissection for the average in vitro length. The in situ lengths among developmental stages were statistically compared using ANOVA with repeated measures, followed by Scheffé's post hoc test ($p<0.05$).

Spinal cords were immediately transferred to a custom-built device that enabled reproducible, quasistatic stretch of tissue in a buffered saline bath. The ends of the spinal cords were clamped, the gauge length between the clamps was measured with digital calipers and recorded, and the spinal cord was restored to the original in situ length, and photographed digitally. The spinal cord was stretched to a stretch ratio (λ) of 1 (unstretched control), 1.05. 1.1, 1.5, or 1.2, where λ is defined as

$$\lambda = \frac{\text{Final Spinal Cord Length}}{\text{Initial Spinal Cord Length}} \tag{1}$$

The spinal cords were then photographed in their stretched state. Three spinal cords were tested for each developmental stage at each level of stretch. Following stretch, the saline was replaced with 4% paraformaldehyde to fix the spinal cord in its elongated state. A previous study demonstrated that fixation did not affect the morphological appearance of undulation [17]. Spinal cords were fixed in their stretched state for 30 min, removed from the device, and re-measured to ensure that the stretched length remained the same. Spinal cords were post-fixed in 4% paraformaldehyde overnight and then incubated in a 20% sucrose-saline solution for at least 24 h for cryoprotection as preparation for immunohistochemical labeling of axons.

Immunohistochemistry. Frozen horizontal sections (10 μm) were cut on a cryostat (Thermo Electron, Pittsburgh, PA) and placed on pre-treated glass microslides (Fisher Scientific, Hampton, NH). Sections were rinsed in buffered solution (1% bovine serum albumin (BSA - Sigma, St. Louis, MO), 0.5% TritonX-100 (Sigma) in phosphate buffered saline (PBS - Sigma)) for 5 min, then incubated in a 10% solution of goat serum (Atlanta Biologicals, Lawrenceville, GA) for 1 h. Sections were then incubated overnight in a 1:1000 dilution of mouse α-neurofilament-200 (Sigma). The next day, sections were washed with buffer four times for 5 min apiece, and then incubated in a 1:400 dilution of Alexa 488 goat anti-mouse secondary antibody (488 nm/515 nm excitation/emission, Molecular Probes, Eugene, OR). Sections were again rinsed (4×5 min), and slides were coverslipped (VECTASHIELD® mounting medium for fluorescence, Vector Labs, Burlingame, CA).

Separate, unstretched spinal cords were harvested similarly and sectioned coronally or horizontally (10 μm) for immunohistochemical labeling of myelin. Sections were double-labeled with a 1:400 dilution of rabbit anti-myelin basic protein (MBP) (Accurate Chemical Scientific, Westbury, NY), as well as the 1:1000 dilution of mouse α-NF-200, followed by incubation in goat anti-rabbit Alexa 488 to visualize the MBP and goat anti-mouse Alexa 546 (568 nm/603 nm excitation/emission) to visualize the neurofilaments. A gross estimate of the degree of myelination in these samples was determined by thresholding images and calculating the ratio the area of myelin immunostaining to neurofilament immunostaining in the white matter. At least two separate sections from three immunolabeled spinal cords were used to identify the average degree of myelination.

Experimental Tortuosity Characterization. Composite images of spinal cord sections from C4/5–T4/T5 were generated with Olympus Microsuite™ software controlling an Olympus IX81 inverted epifluorescent microscope (Olympus, Melville, NY) and a Hamamatsu ORCA 285 digital camera (Hamamatsu City, Japan). Individual axonal segments in the lateral funiculus that spanned at least several periods of undulation were identified at random. Two measurements were made for each axonal segment with the Microsuite™ software. The actual pathlength was

Downloaded From: https://biomechanical.asmedigitalcollection.asme.org on 04/23/2019 Terms of Use: http://www.asme.org/about-asme/terms-of-use

found by tracing the segment with the cursor. The end-to-end length was then identified from the coordinates of the beginning and end of the traced line. Each segment was considered an independent sample. These two measurements were made for several hundred randomly located axons for each spinal cord, and the results tabulated in a database. The tortuosity of each axon was then calculated as:

$$T = \frac{\text{actual length}}{\text{end-to-end length}} = \frac{L_A}{L_E} \tag{2}$$

Tortuosity distributions were compared statistically using a Kruskal-Wallis (K-W) non-parametric test for comparison among development days and stretch levels (when more than two conditions were being compared), followed by pairwise Kolmogorov-Smirnov (K-S) non-parametric tests (SPSS, Chicago, IL). Significance values were set at $p < 0.05$.

Mathematical Modeling. To evaluate the nature of the microkinematic response of spinal cord axons to stretch, the control, unstretched tortuosity values for each embryonic stage were used as input data into Matlab® scripts (Mathworks, Inc, Natick, MA) based on previously developed affine and non-affine models of axonal kinematics to predict tortuosity distributions at the various stretch levels in idealized cases [17]. The actual distributions were then compared to the idealized extremes to discern affine and/or non-affine trends in the experimental data. These models have been previously presented [17] and are briefly reviewed.

Affine Model. In the affine model, spinal cord axons are assumed to be tightly interconnected, such that individual axons experience the same geometric transformation as the macroscopic tissue. The geometry of an undulated axon is modeled as a periodic wave with amplitude A_o and period P_o:

$$y(z) = A_o \cos\left(\frac{2\pi z}{P_o}\right) \tag{3}$$

During simple extension of the spinal cord, the amplitude and period of an axon become $A_o(\lambda)^{-1/2}$ and $P_o\lambda$, respectively, and the equation of the stretched axon's geometry changes accordingly:

$$y'(z) = \frac{A_o}{\sqrt{\lambda}} \cos\left(\frac{2\pi z}{\lambda P_o}\right) \tag{4}$$

The transformed tortuosity T_t of the axon is determined by calculating L_A from the pathlength of Eq. (4) from 0 to L_E, and dividing by L_E:

$$T_t = \frac{1}{L_E}\int_0^{L_E} \sqrt{1 + \left[\frac{-A_o}{\sqrt{\lambda}}\frac{2\pi}{\lambda P_o}\sin\left(\frac{2\pi z}{\lambda P_o}\right)\right]^2}\, dz \tag{5}$$

which is approximated with a simplification that applies for undulation values close to 1.0 [17].

$$T_t = T_o\left[\frac{1}{\lambda^3} + \frac{1}{T_0^2}\left(1 - \frac{1}{\lambda^3}\right)\right]^{\frac{1}{2}} \tag{6}$$

This approximation generates only 0.3% error at a stretch ratio of 1.5, which is far greater than the maximum stretch employed in this study ($\lambda_{max} = 1.2$).

Non-affine Model. When axons within the white matter of the spinal cord are assumed to be completely uncoupled to each other, the microstructural transformation is calculated directly from the original tortuosity and the applied stretch ratio [17]:

$$T_t = \frac{1}{\lambda}T_o \quad \text{for } \lambda < T_o \tag{7}$$

An axon is completely straight when the tissue stretch ratio (λ) is equal to the axon's original undulation (T_0), after which by definition:

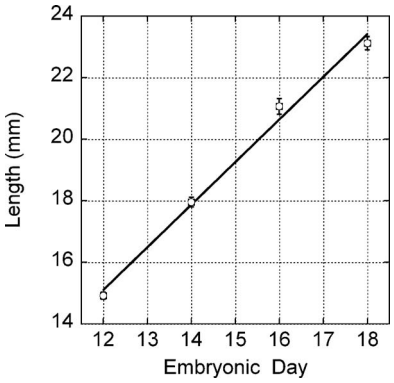

Fig. 1 Chick embryo spinal cord growth in ovo from E12 to E18. During this period of development, the length between the third to thirteenth nerve root increased almost 55%. Significant increases in length were observed from stage-to-stage (ANOVA with repeated measures, followed by Scheffé's post hoc tests, max $p < 0.001$). Growth during this period was linear ($R^2 = 0.99$), with a slope (± std err) of 1.38 ± 0.02 mm/day.

$$T_t = 1 \text{ for } \lambda \geq T_o \tag{8}$$

Using these transformations, tortuosity distributions were predicted for the control populations of axons from the chick embryo spinal cords at different stages of development subjected to increasing levels of controlled, uniaxial stretch.

"Switching" Model. In previous work with the guinea pig optic nerve, a switching model, where axon kinematic behavior gradually shifted from non-affine to affine behavior, was employed [1]. Three regimes were defined:

- Regime 1: $T < T_1$ Affine behavior
- Regime 2: $T > T_2$ Non-affine behavior
- Regime 3: $T_1 <= T <= T_2$ Potential transition from non-affine to affine behavior

An axon with tortuosity that falls in regime 1 will demonstrate fully coupled behavior, whereas an axon with tortuosity that falls in regime 2 will demonstrate fully uncoupled behavior. When an axon's tortuosity falls in regime 3, it is capable of switching from uncoupled to coupled behavior. The transition point is uniquely defined for each axon by selecting a tortuosity value at random that falls between T_1 and T_2, based on a uniform distribution. Therefore, the values of T_1 and T_2 define the transition behavior for the group of axons. These values were estimated for each developmental stage by minimizing the net difference between experimental and predicted histograms across all stretch levels using a Levenberg-Marquardt multi-parameter, non-linear regression scheme [31]. Since the switching model involves the random assignment of a particular transition tortuosity to a given axon, the optimization was executed 50 times for each developmental stage, from which the mean transition values and standard deviations were determined.

Results

Growth of Chick Embryo Spinal Cord. From E12 to E18, significant increases were observed in the growth of the chick embryo spinal cord between each of the measured stages (ANOVA with repeated measures, followed by Scheffé's post hoc test, max $p < 0.001$) (Fig. 1). During this time, the length of spinal cord between the 11 nerve roots increased almost 8 mm. Spinal cords did not shrink following excision of the whole spinal column from the chick, but did consistently decrease in length ~5% following removal of the vertebrae and full excision from the spinal column, indicating a level of in vivo tension. No statistical

Downloaded From: https://biomechanical.asmedigitalcollection.asme.org on 04/23/2019 Terms of Use: http://www.asme.org/about-asme/terms-of-use

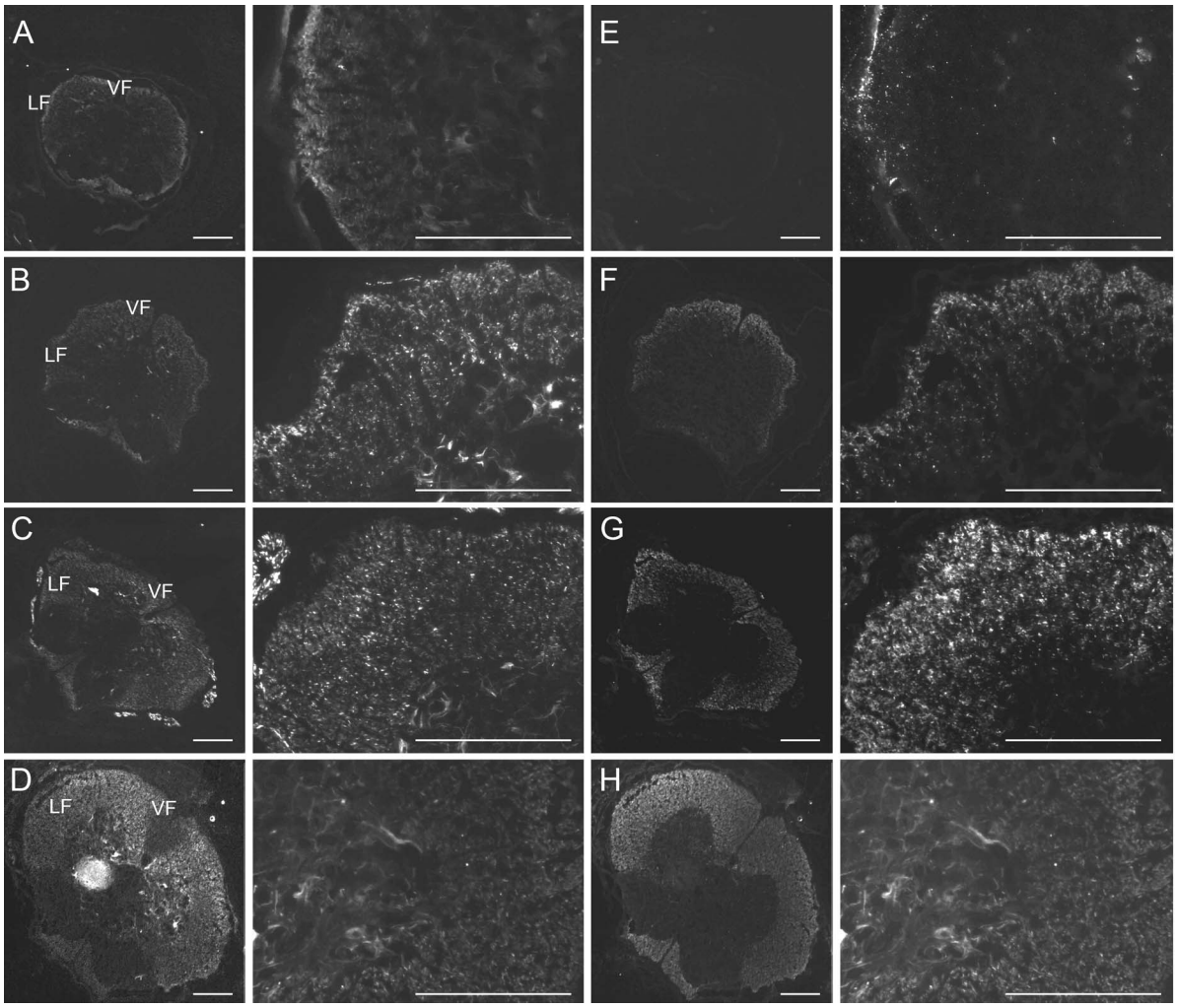

Fig. 2 Progression of myelination in the chick embryo spinal cord. (*A–D*) Neurofilament immunohistochemistry indicating presence of axons. (*E–H*) Myelin basic protein immunohistochemistry indicating myelination. Low magnification images of whole cross sections and higher magnification images of the lateral funiculus (LF) were taken following immunohistochemical double-labeling of the chick embryo spinal cord. Little myelin was observed in E12 spinal cords (*E* versus *A*). At E14 (F versus B), myelination is pronounced in the ventral funiculus (VF), but less so in the lateral funiculus. By E16 (*G* versus *C*), myelination has begun in nearly all white matter tracts, and by E18 (*H* versus *D*) myelin is pronounced throughout the white matter, including the lateral funiculus. Scale bars=200 μm.

trends relating the percentage of tissue shrinkage to development stage were observed. The spinal cords were restored to the in situ length prior to fixation and sectioning.

Immunohistochemistry. Digital imaging following immunolabeling of neurofilaments with α-NF200 revealed many continuously labeled axons that were easily viewed with epifluorescence microscopy at all stretch levels. The progression of myelination was confirmed with immunolabeling of MBP (Fig. 2). The degree of myelination, which was estimated by determining the ratio of myelin immunolabeling to neurofilament immunolabeling in cross sections and horizontal sections, steadily increased from E12–E18 (ANOVA, followed by Scheffé's post hoc test, max $p=0.008$), with the largest increase occurring between E14 and E16 (Fig. 3).

Tortuosity Characterization of Axons in Unstretched and Stretched Spinal Cords. Axons in unstretched, control spinal cords were visibly undulated, and became noticeably straighter with increasing stretch ratio. From these images, axonal pathlengths and end-to-end lengths were identified with Olympus Microsuite™ Software to quantitatively characterize axonal tortuosity changes with development and with stretch. Representative images and associated tortuosity distributions are presented for E12 spinal cords in Fig. 4. Normalized distributions for all embryonic stages and stretch levels are shown in Fig. 5, and summary statistics of the tortuosity characterization are presented in Table 1. Tortuosity distributions in E12 unstretched spinal cords could not be statistically distinguished from a normal distribution (K-S test versus normal distribution, $p=0.192$), but those from E14, E16, and E18 were significantly different (max $p=0.014$), and generally resembled the distribution of axons in the unstretched guinea pig optic nerve [17]. With stretch, the distributions changed markedly, but the nature of the changes depended upon the developmental stage. Statistical analysis of axonal tortuosity in control, unstretched spinal cords revealed significant changes in tortuosity distributions with development among all stages (K-W test, $p<0.001$), and from E12 to E14 ($p=0.001$) and E14 to E16 ($p=0.001$) (K-S test). Tortuosity distributions from unstretched E16 and E18 spinal cords were not significantly different (K-S test, $p=0.177$). Tortuosity generally decreased with increasing development. Among all stages and within each stage, stretch significantly decreased tortuosity ($p<0.001$, K-W test followed by K-S tests for pairwise testing of stretch levels). The following pairwise comparisons were not significant (K-S test):

Downloaded From: https://biomechanical.asmedigitalcollection.asme.org on 04/23/2019 Terms of Use: http://www.asme.org/about-asme/terms-of-use

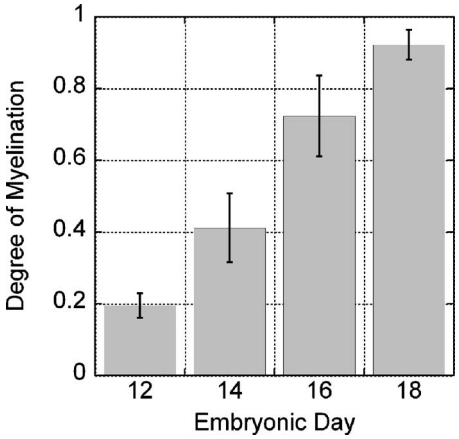

Fig. 3 Quantitative comparison of changes in myelination with development. The degree of myelination was determined from images of immunohistochemically double-labeled spinal cord tissue as the ratio of myelin-positive staining to neurofilament-positive staining in white matter. The degree of myelination (average ± standard deviation) increased significantly from E12 to E18 (ANOVA, followed by Scheffé's post hoc test, max $p=0.008$).

E12 versus E14, 10% stretch ($p=0.519$); E12 versus E18, 5% stretch ($p=0.139$); and E14 versus E16, 5% stretch ($p=0.055$). All other pairwise comparisons were significant. (max $p=0.042$).

Interpretation of Model Results. Before presenting the results of the affine, non-affine, and switching models, it is helpful to describe the impact of the bounds of the transition tortuosity (T_t) distribution, T_1 and T_2, on the results of the switching model (Figs. 6 and 7). In Fig. 6, frequency and cumulative frequency distributions are presented where T_1 is varied from 0.8-1.2 while T_2 is held constant at 1.4. Prior to stretch, if $T_{axon}<T_t$, then the axon has already switched, and it will exhibit affine behavior from the onset. If $T_{axon}>T_t$, the axon will exhibit non-affine behavior during stretch until $T_{axon}=T_t$. Thus, as T_1 increases, axons exhibit more affine behavior. Importantly, when $T_1<1$, a percentage of the axons $((1-T_1)/(T_2-T_1))$ will have transition tortuosities less than 1. Since the actual tortuosity of an axon has a lower bound of 1 (perfectly straight), any axon with $T_t<=1$ will always exhibit non-affine behavior, because $T_{axon}>T_t$ will always hold. Thus, as T_1 decreases below 1 (holding T_2 constant), more axons will permanently exhibit non-affine behavior. This is seen as an increase in the fraction of axons with tortuosity of (or very close to) 1, as more axons with lower initial tortuosities become perfectly straight; axons with higher initial tortuosities are relatively unaffected.

Figure 7 depicts the influence of changing T_2 (the upper bound of the transition tortuosity distribution) on axon behavior while holding T_1 constant for 10% stretch. As T_2 decreases, more axons will have $T_{axon}>T_t$, so we will again see a shift towards non-affine behavior. This will generally affect axons with higher initial tortuosities, so the influence of changing T_2 is more evident at the upper end of the tortuosity distributions. We also note that the distribution used for the initial population has a mean tortuosity of ~1.08 to generally match the distributions of axons from unstretched spinal cords in our study; therefore, transition zones that operate towards lower values of tortuosity will naturally influence a larger percentage of actual axons.

Kinematic Models of Axon Behavior. The affine, non-affine, and switching models were compared to the experimental data for all embryonic stages (see Figs. 8 and 9 for representative results from E12 and E18, respectively). The tortuosity data from multiple samples were pooled by developmental stage and stretch level. Pooled control data for each developmental stage was used as input data into the kinematic models to predict tortuosity changes for these idealized extreme descriptions of microkinematic behavior. Neither the affine nor the non-affine model matched the experimental data at any developmental stage. However, experimental tortuosity distributions clearly shifted from more non-affine behavior at early developmental stages (E12, E14) to more affine at later stages (E16, E18), especially at lower magnitudes of stretch. In comparison, for all developmental stages, the switching model greatly improved the predictive capacity of the model. Because the switching model involved randomly assigning a transition tortuosity to each axon from a uniform distribution, the model was executed 50 times for each developmental stage. In each run, the values of T_1 and T_2 were optimized by regressing the predicted tortuosity distributions against the experimental data across all stretch levels (Fig. 10). Average regression coefficients were: 0.94±0.005 for E12; 0.95±0.003 for E14; 0.93±0.007 for E16; and 0.86±0.01 for E18. For all stages, $T_1<1$ and $T_2>1$, indicating that a fraction of the axons exhibited pure non-affine deformation at each stage. This percentage significantly decreased (ANOVA, $p<0.001$) with development as follows: 65.0% ±1.9% for E12; 60.7% ±2.0% for E14; 39.7% ±4.5% for E16; and 29.4% ±1.5% for E18. The values for T_1 increased significantly from E12 to E18 (ANOVA followed by pairwise comparisons with Scheffé's post hoc test, $p<0.001$), with the steepest increase between E14 and E16. Conversely, though statistically significant differences were observed among all stages (ANOVA, $p<0.01$), pairwise post hoc tests (Scheffé's test) revealed no discernable trends for T_2 with development. Another set of simulations was run where T_2 was fixed at the average value across the four stages (1.087) and only T_1 was determined through non-linear regression. The values and trend for T_1 from the one-parameter fit were statistically indistinguishable from T_1 values from the 2-parameter fit. (ANOVA, $p=0.37$).

One final set of simulations was performed to evaluate the potential influence of physical strain imparted on the spinal cord during growth as the basis for the transition from predominantly non-affine to predominantly affine kinematics during development. It was assumed that the change in length from E12 to E18 could be modeled, at an extreme, as an incrementally applied stretch with the length at E12 serving as the gauge length. The kinematic models were executed for three stretch levels representing the incremental growth from E12 to E14 ($\lambda=1.20$), E12 to E16 ($\lambda=1.41$), and E12 to E18 ($\lambda=1.55$), and the results were compared to E14, E16, and E18 control distributions, respectively. Similar simulations were executed for growth/stretch from E14 to E16, E14 to E18, and E16 to E18. As shown in Fig. 11, both non-affine and affine models grossly under-predicted the tortuosity that was measured in the unstretched controls. (The switching model naturally falls between the affine and non-affine models.)

Discussion

In this study, we investigated how deformation of the underlying axonal microstructure of spinal cord white matter changes during a period of rapid growth and initiation of myelination to begin to examine how coupling of axons to the glial matrix influences deformation behavior. To evaluate the mechanical behavior, we took advantage of the tortuous, undulated nature of axons in normal white matter [16]. A previous study by Bain et al. described general methods to quantitatively characterize axonal tortuosity in central nervous system white matter (the guinea pig optic nerve), and demonstrated that undulated axons straighten as macroscopic stretch is applied to the white matter [17]. That study also compared the changes in axonal tortuosity that resulted from straightening during stretch to mathematical predictions of ideal affine and non-affine behavior. It was concluded that neither model described the experimental data perfectly, and that axon mechanics in the guinea pig optic nerve appeared to transition

Downloaded From: https://biomechanical.asmedigitalcollection.asme.org on 04/23/2019 Terms of Use: http://www.asme.org/about-asme/terms-of-use

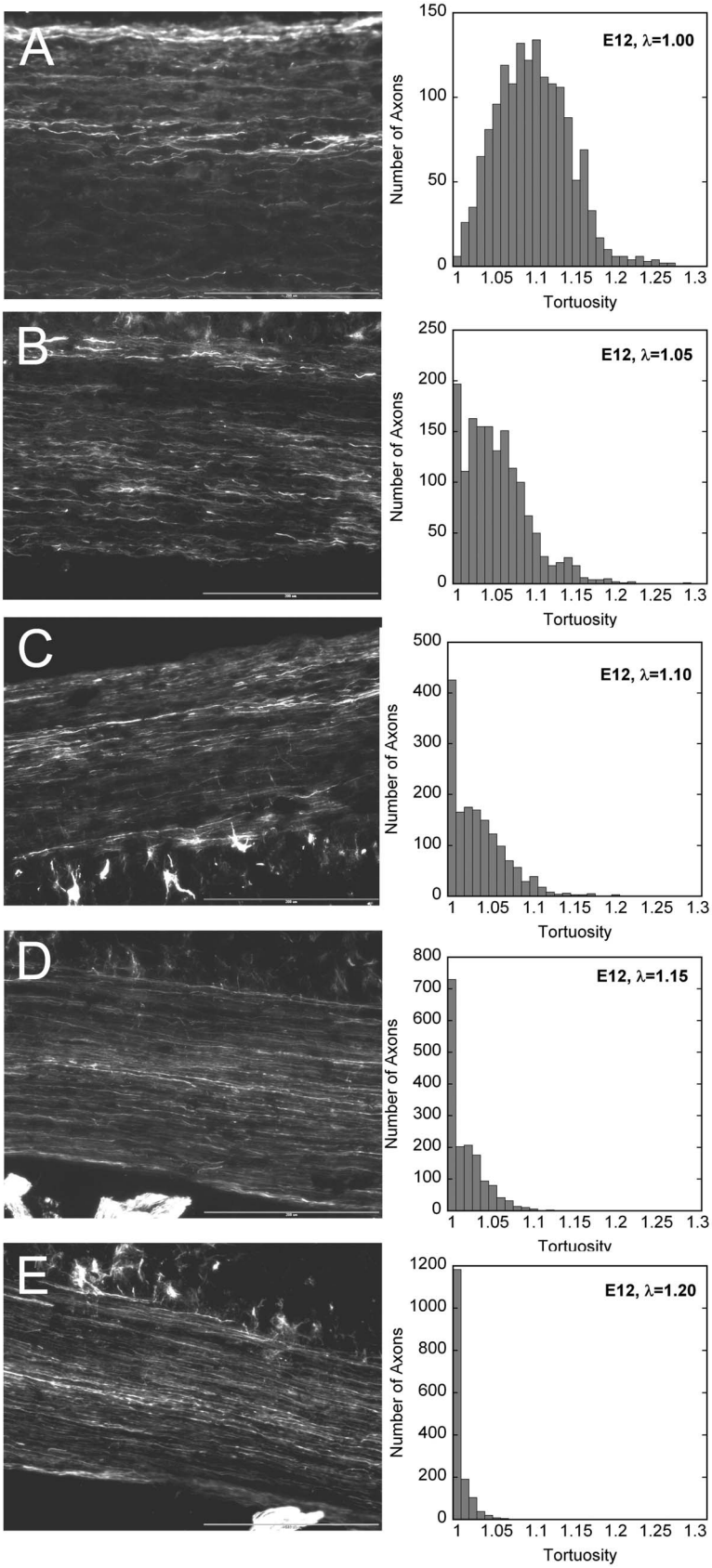

Fig. 4 Immunohistochemistry and tortuosity characterization for E12 spinal cords. Fixed spinal cords were sectioned horizontally and immunhistochemically stained for neurofilament proteins. (*A*) Many axially oriented, wavy axons were observed in unstretched spinal cords. The distribution of axonal tortuosity followed a normal distribution. As stretch increased ((*B*)=5%, (*C*)=10%, (*D*)=15%) axons became progressively straighter, and a significant number of axons had tortuosity equal or near one. At the highest stretch ratio ((*E*)=20%), almost all axons appeared to be straight or nearly straight. (Scale bars=200 μm.)

Downloaded From: https://biomechanical.asmedigitalcollection.asme.org on 04/23/2019 Terms of Use: http://www.asme.org/about-asme/terms-of-use

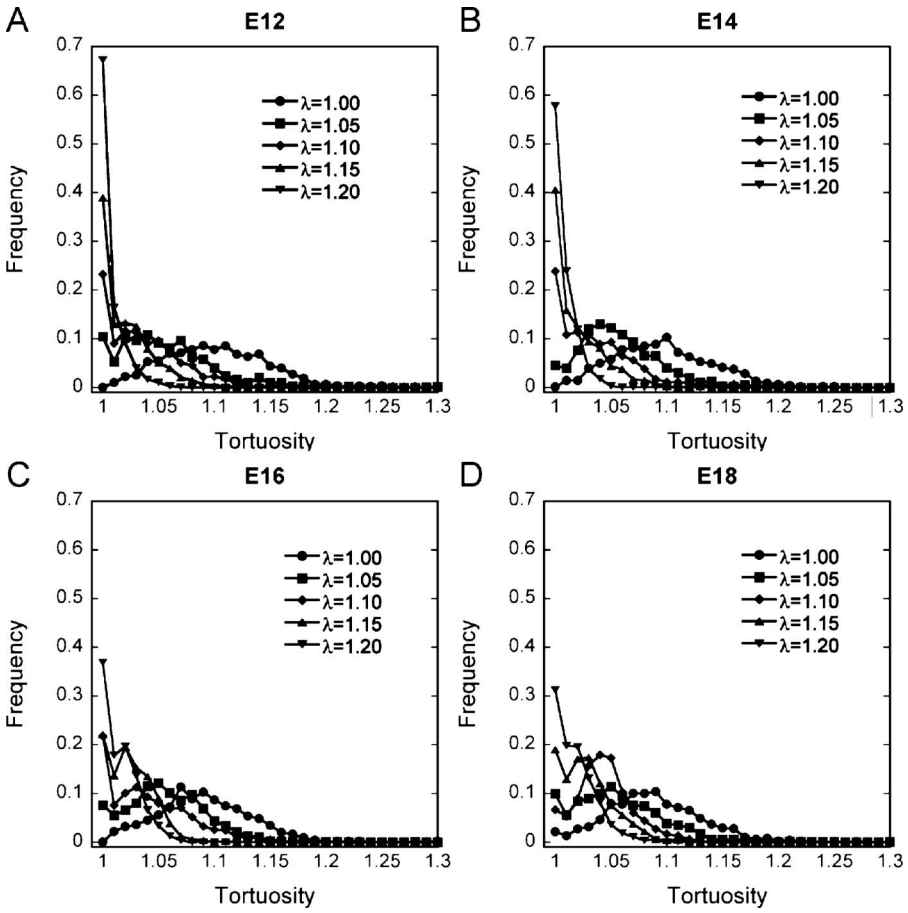

Fig. 5 Normalized axonal tortuosity distributions following controlled stretch for (*A*) E12, (*B*) E14, (*C*) E16, and (*D*) E18 chick embryo spinal cords. Each embryonic stage demonstrated similar distributions in unstretched spinal cords and as stretch was increased. The peak of the distributions for unstretched cords (circles, λ=1) shifted left from E12 to E18, indicating a progressive straightening of axons with growth and development. With increasing stretch, E12 axon tortuosity demonstrated a pronounced shift to the left (in a left-censored fashion), such that at 20% stretch, over 60% of the axons had a tortuosity ~1, and a sharp drop-off in the distribution followed (inverted triangles, λ=1.20). With growth and development, distributions shifted to the left to lesser degrees, such that at E18, just over 30% of the axons had a tortuosity ~1, and the subsequent fall-off was less steep.

Table 1 Summary statistics for tortuosity measurements

Development stage	Stretch level	Mean tortuosity	Standard deviation	Total number of axons
E12	0%	1.096	0.046	1553
	5%	1.051	0.042	1531
	10%	1.033	0.034	1556
	15%	1.012	0.021	1599
	20%	1.004	0.010	1552
E14	0%	1.092	0.044	1523
	5%	1.052	0.035	1524
	10%	1.034	0.042	1580
	15%	1.017	0.028	1530
	20%	1.005	0.009	1544
E16	0%	1.085	0.041	1523
	5%	1.052	0.035	1532
	10%	1.038	0.037	1536
	15%	1.021	0.021	1582
	20%	1.012	0.014	1558
E18	0%	1.083	0.043	1561
	5%	1.051	0.039	1552
	10%	1.040	0.026	1533
	15%	1.025	0.023	1522
	20%	1.014	0.017	1527

from non-affine behavior at low stretch levels to affine behavior at high stretch levels. It was proposed that coupling to the glial matrix was responsible for this transition. Based on these observations, we believed that the degree of interconnectivity of axons via the glial matrix would be demonstrated as a transition from predominantly non-affine to affine behavior during myelination of the white matter, where interconnections via the glial matrix are being established, primarily via oligodendrocytes but also via astrocytes. We also wanted to examine the response of other white matter that is more often injured during trauma. We therefore characterized the kinematic response of axons to controlled stretch in the developing chick embryo spinal cord during a period of rapid myelination.

Chick embryo spinal cord axons exposed to controlled stretch generally followed the same trends as adult guinea pig optic nerve axons, demonstrating a transition from non-affine mechanics at low stretch levels to affine mechanics at high stretch levels. As expected, non-affine, uncoupled behavior was more prevalent earlier in development, and affine, coupled behavior increasingly prevailed later in development, though at no stage was behavior purely non-affine or affine. This trend was quantified by employing the "switching" model proposed by Bain et al. [17], where each axon is assumed to exhibit non-affine behavior and

Downloaded From: https://biomechanical.asmedigitalcollection.asme.org on 04/23/2019 Terms of Use: http://www.asme.org/about-asme/terms-of-use

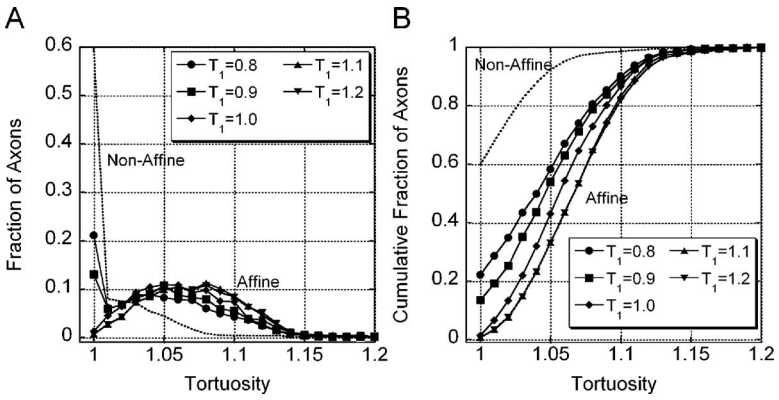

Fig. 6 Effects of changing T_1 on predicted tortuosity distributions of E14 control axons exposed to 10% stretch. T_1, which represents the lower bound of the uniform distribution that defines the switching parameters, was varied from 0.8 to 1.2, while holding T_2 constant at 1.4. T_1 influences the left-hand side of the tortuosity distribution. Increasing T_1 shifts the behavior from non-affine to affine.

straighten directly with stretch until its tortuosity decreases to a transition tortuosity (prescribed at random from a uniform distribution), after which it demonstrates affine behavior. Using a nonlinear regression scheme, we identified the bounds of the uniform distribution that described the transition tortuosity for each developmental stage. The lower bound (T_1) showed progressive, significant increases from 0.84 at E12 to 0.96 at E18. Though significant differences in the upper bound were detected, no trends in the value of the upper bound with development were discerned (average $T_2=1.087$). Significant percentages of each uniform, transition distribution were below a transition tortuosity of 1. This percentage represents the fraction of axons whose transition tortuosity will never be reached (since the lower bound on tortuosity is 1). Thus, these axons can never switch from non-affine to affine behavior. The percentage of axons predicted to demonstrate solely non-affine behavior decreased during the developmental period studied (64% at E12, 60% at E14, 39% at E16, and 30% at E18), again representing a switch from uncoupled to coupled behavior with development. These values were well correlated (negatively) with both average developmental changes in length ($R^2=0.938$) and degree of myelination ($R^2=0.970$). Interestingly, the T_2 value in our study, which was insensitive to changes with development, compared very favorably with upper bound in determined in the guinea pig optic nerve study ($T_2=1.08$), while the lower bound from the optic nerve study ($T_1=0.98$) was slightly greater than T_1 for E18 spinal cords, and agreed nicely with the trend of increasing T_1 with development discerned in our study (assuming the adult guinea pig optic nerve is "fully myelinated").

In both the study by Bain et al. [17] and the current study, axon tortuosity is measured within the two-dimensional plane that is imaged, and it is modeled as a 2D sinusoidal wave. We took special care to orient the spinal cord consistently with the ventral side down during sectioning to evaluate tortuosity in the same plane across samples. However, the axon likely traverses through the thickness of the plane as well, though it is not clear if the axon maintains a regular helix around the long axis, if there is a lower order meander, or if there is merely random changes in the orientation of waviness. In any case, approximating the 3D tortuous path of the axon with its 2D projection underestimates the actual pathlength of the axon, but maintains the end-to-end length, thereby underestimating the tortuosity of the axon. Approximating the "3D" axon as a coil with an amplitude that is 10% of the period, which roughly matches the unstretched, E12 axons, results in an 8% increase in the predicted tortuosity when the 3D path is considered. This error increases as the axons become wavier (or more coiled). We would expect this to be systematic error and not

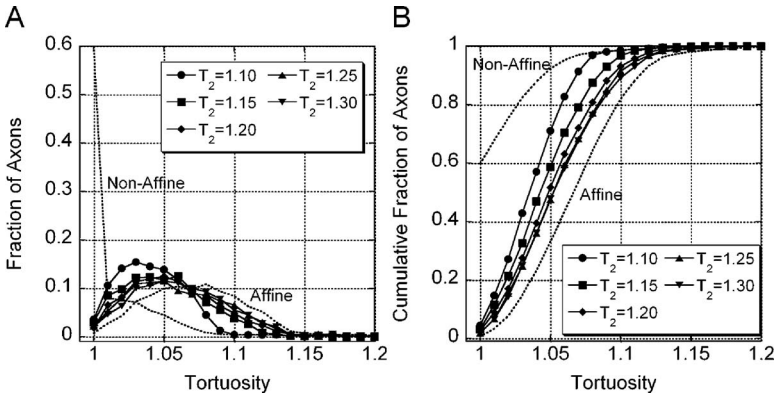

Fig. 7 Effects of changing T_2 on predicted tortuosity distributions of E14 control axons exposed to 10% stretch. T_2, which represents the upper bound of the uniform distribution that defines the switching parameters, was varied from 1.1 to 1.3, while holding T_1 constant at 1.0. T_2 influences the right-hand side of the tortuosity distribution. Increasing T_2 shifts the behavior from non-affine to affine.

Downloaded From: https://biomechanical.asmedigitalcollection.asme.org on 04/23/2019 Terms of Use: http://www.asme.org/about-asme/terms-of-use

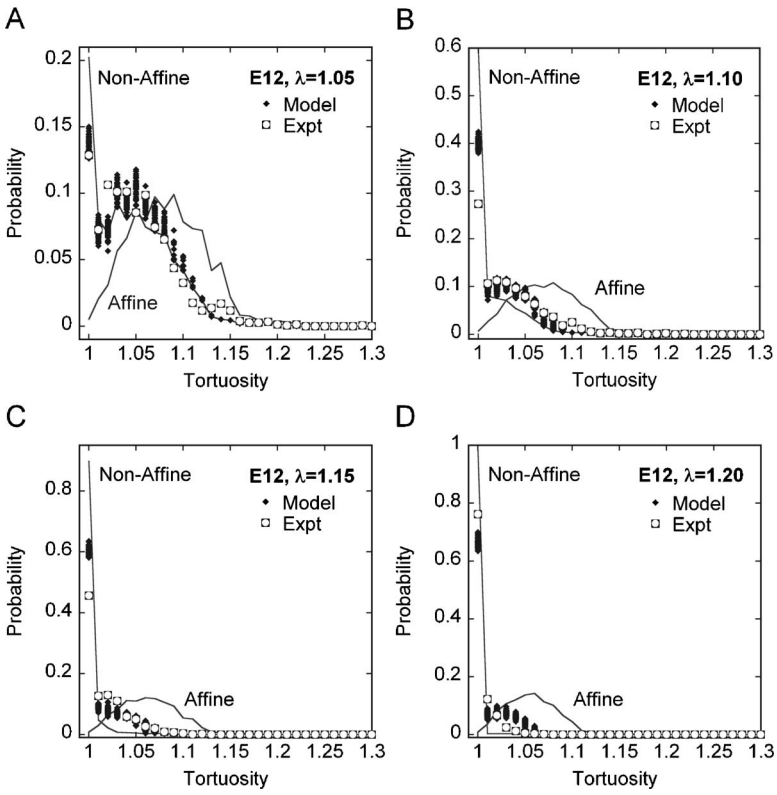

Fig. 8 Comparison of E12 results to affine, non-affine, and switching kinematic models. Neither the affine nor non-affine model (solid lines) suitably matched the experimental data (open squares) describing tortuosity changes with tissue level-stretch ((*A*)–5%. (*B*)–10%. (*C*)–15%, (*D*)–20%), though the general trend was better predicted by the non-affine model. The experimental data across all stretch levels was used as the objective function to optimize the switching model. The non-linear regression was executed 50 times (diamonds). The optimized switching model provided a much improved prediction of tortuosity (average $R^2 = 0.94 \pm 0.0015$ for the 50 simulations).

to change with growth/development, although we are investigating methods to extract and measure the 3D pathway in an efficient manner for 3D tortuosity characterizations.

Many changes occur in chick embryo spinal cord white matter during the development period studied. In addition to myelination, the most overt change is the dramatic increase in length of the spinal cord—almost 55% in 6 days—that occurs as the chick grows in size. This increase in the length of the spinal cord results from mechanical force placed on spinal cord tissue by the growing skeleton. Mechanical force placed directly on neurite growth cones causes axon lengthening via a "towed-growth" mechanism [32–35], and has shown to increase the length of internodal segments in peripheral nerves [36]. Since in both the present study and in Bain et al. [17] there was a clear transition of kinematic behavior during stretch, it is possible that the stretch experienced during physical growth straightens axons in the spinal cord and is responsible for the observed transition from non-affine to affine kinematics during development. This is akin, at the extreme, to stating that any imposed stretch ex vivo is added on to the stretch experienced during growth in vivo, so that growth can be expected to significantly decrease the average tortuosity and, essentially, cause many axons to reach their transition tortuosity and switch from non-affine to affine behavior.

Indeed, as the spinal cord grew from E12 to E18, we observed a modest but significant decrease in tortuosity, as well as an increase in the number of "perfectly straight" axons, which essentially represents a shift in the tortuosity distribution towards straighter axons (a "left-censored" distribution) [37]. However, the degree to which the axon population straightened as a result of growth-induced tissue stretch was far less than that predicted by any of the kinematic models examined (Fig. 11). Assuming the appropriate switching parameters, T_1 and T_2, from the in situ characterizations, the model predicts that the decreases in tortuosity from E12 to E14, E14 to E16, and E16 to E18 result from stretch ratios of $\lambda = 1.004$, $\lambda = 1.0065$, and $\lambda = 1.0032$, respectively, which are minimal compared to the percent increase in growth (20%, 17%, and 10%, respectively). Thus, we conclude that tissue stretch during growth contributes minimally to the overall kinematic behavior. Furthermore, we infer from this observation that there is an inherent mechanism to preserve axon tortuosity as the axons grow during development, perhaps to provide slack as a neuroprotective measure. Although the tensile stress/strain applied during growth is presumably uniaxial, new axoplasm, cytoskeletal elements, and axolemma are either generated in a tortuous geometry or are contracted to that geometry by other cells, such as oligodendrocytes, or by active contraction of axonal cytoskeletal elements. There is evidence of some contractile machinery in axons that allows them to recover from large strains experienced in vitro to return to an "original" length, even following elongation of over 60%, which was coined "delayed elasticity" by Smith et al. [38]. It is possible that the same machinery operates in vivo to contract axons following growth-induced extension.

In addition to lengthening, several other changes occur during the development period studies, such as the formation of new axon tracts, maturation of existing tracts, and vasculogenesis.

Downloaded From: https://biomechanical.asmedigitalcollection.asme.org on 04/23/2019 Terms of Use: http://www.asme.org/about-asme/terms-of-use

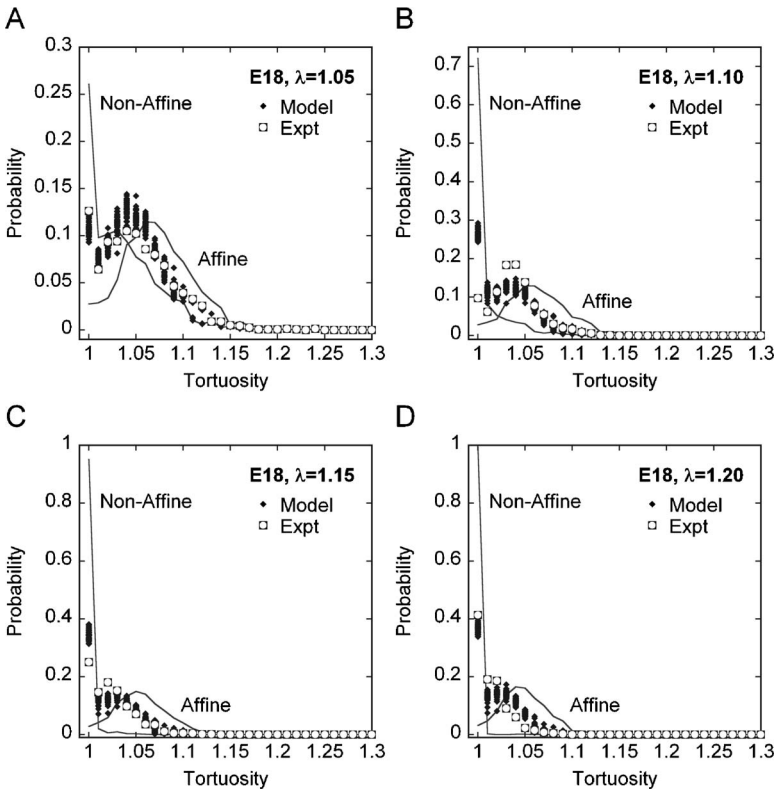

Fig. 9 Comparison of E18 results to affine, non-affine, and switching kinematic models. Neither the affine nor non-affine model (solid lines) suitably matched the experimental data (open squares) describing tortuosity changes with tissue level-stretch ((*A*)–5%. (*B*)–10%. (*C*)–15%, (*D*)–20%), though, like E16, the shift from non-affine to affine kinematics with stretch was more obvious. The experimental data across all stretch levels was used as the objective function to optimize the switching model. The non-linear regression was executed 50 times (diamonds). The optimized switching model provided a much improved prediction of tortuosity (average R^2 =0.86±0.01 for the 50 simulations).

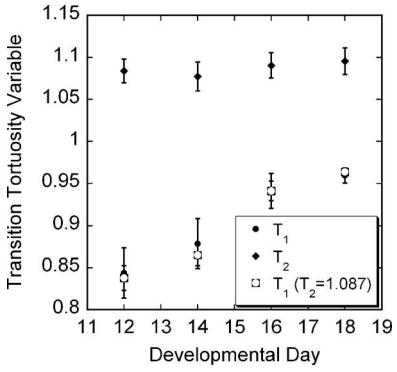

Fig. 10 Upper and lower bounds of the uniform distribution defining the best-fit switching models for all developmental stages (average ± standard deviation of the 50 simulations per stage). For all stages, $T_1<1$ and $T_2>1$, indicating that a percentage of the axons $[(1-T_1)/(T_2-T_1)\times 100]$ demonstrates solely non-affine kinematics. Though statistical differences were detected among T_2 values (diamonds), (ANOVA, $p<0.01$), no consistent trend was observed with developmental stage. Conversely, T_1 (circles) increased with developmental stage, and showed the greatest increase between E14 and E16. A second set of simulations were run to find the values of T_1 while holding T_2 fixed across developmental stages at the average value from the two-parameter fits (T_2=1.087). T_1 values from the one-parameter fit (open squares) were not significantly different than T_1 values from the two-parameter fit (p=0.37).

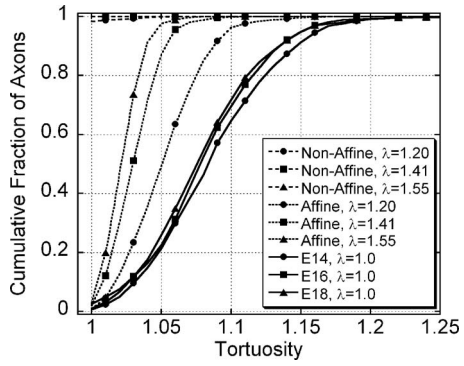

Fig. 11 Predicted tortuosity cumulative distributions when applying incremental stretch to E12 control axons to simulate growth-induced stretch of the spinal cord. The percentage increases in length from E12 to E14, E12 to E16, and E12 to E18 were used as the applied stretch in the kinematic models, and the results were compared to unstretched distributions from E14, E16, and E18, respectively. All three kinematic models grossly over-estimated the degree of straightening that would be produced by growth of the spinal cord. (The switching model falls naturally between the non-affine and affine models and is not shown.) Similar results were observed following simulation of growth from E14 to E16, E14 to E18, and E16 to E18.

Downloaded From: https://biomechanical.asmedigitalcollection.asme.org on 04/23/2019 Terms of Use: http://www.asme.org/about-asme/terms-of-use

However, the maturation of oligodendrocytes and subsequent myelination of axons represents the primary morphological change in the tissue, and, therefore, the most likely source of coupling behavior. Our technique enabled gross evaluation of myelination based on image analysis of low magnification images. The degree of myelination in our study is advanced compared to the previous characterization of myelination in the ventral funiculus, where myelination was documented for individual axons using a combination of immunohistochemistry and electron microscopy. However, the trends match reasonably well, and show a sigmoidal time course of myelination, with the linear portion occurring between E14 and E16 [29]. This is also where we see the sharpest increase in T_1 and an associated increase in coupled behavior. Herein, we have studied axon kinematics in the normally developed chick embryo spinal cord and have not attempted to control myelination as an independent variable. Thus, we can only say that the observed change in axonal mechanics during development correlates with increased myelination. Based on these observations, we are now more directly examining the role of myelin and glia in axon kinematics with a number of techniques that selectively interfere with myelination and/or kill specific glia in ovo. With this approach, we believe it will be possible to tease out the relative influence of astrocytes and oligodendrocytes on axonal coupling.

Increased myelination may influence axon kinematic behavior is several ways. As the volume of myelin increases, so does the potential for increased adhesion among axons at the molecular level [39]; since the volume of myelin differs in different white matter tracts [40], axon kinematics may also be tract-dependent. However, we believe that the change in kinematic behavior is due to axon-axon coupling via oligodendrocytes. Oligodendrocytes may myelinate—and, therefore, physically connect—many axons to act as cellular crosslinks in addition to their role in increasing action potential conduction velocity. The nature of the oligodendrocytes and/or the number of axons it myelinates would then influence the mechanical coupling these cell provide, defining when an oligodendrocyte's process becomes taut enough to couple the motion and deformation of one axon to the next.

In fact, it is well established that oligodendrocyte morphology is related to axon diameter [41,42]. Generally, small diameter CNS axons are myelinated by type I and II oligodendrocytes, and large diameter CNS axons are myelinated by type III and IV oligodendrocytes. Type I and II oligodendrocytes typically myelinate many axons and maintain shorter internodal lengths. Type III and IV oligodendrocytes only myelinate a few axons/segments (and may only myelinate one) with longer internodal distances. Both the type I/II and III/IV oligodendrocytes only myelinate axons of a similar diameter, so large- and small-caliber axons are not myelinated by the same cell [43]. Moreover, areas with a mixture of large and small diameter axons, such as the ventral funiculus, are generally myelinated earlier during development than areas with predominantly small diameter axons, such as the corticospinal tract [44]. Thus, the composition of the population of myelinating oligodendrocytes in the spinal cord varies throughout development, and may affect the nature of axon-axon mechanical coupling. The lateral funiculus is composed of axon fibers from many tracts, including the corticospinal, rubrospinal, and vestibulospinal descending tracts and the posterior spinocerebellar tract that, collectively, represent a mixture of axon sizes and oligodendrocytes types [44,45]. By selecting hundreds of randomly located axons throughout this region spinal cord, we hoped to minimize any regional bias in the type of oligodendrocytes.

Regardless of the mechanism of increased coupling, the observed differences have clear implications for defining tolerances for brain and spinal cord injury. The degree of tortuosity and the axon kinematics combine to dictate how macroscopic, tissue-level strain is transferred to the microstructure to ultimately produce injury [10,17]. Thus, any spatial and/or temporal variations in tortuosity and kinematics during development would affect the injury response. For instance, while myelination of the chick spinal cord may be nearly complete at hatching, myelination of the human spinal cord is incomplete at birth and continues to at least 3 years of age [25], and maturation of white matter fiber tracts (thickening of axons and myelin sheaths) can continue well into adolescence, especially in tracts involved in motor pathways [26]. Hence, the tolerance of human white matter to stretch could very well vary significantly during development. It is known that the mechanical properties of brain tissue change with development [46,47], which would, in turn, affect the injury response of the brain and spinal cord [48]. The changes in microstructural kinematics could contribute to the observed changes in macroscopic tissue mechanical behavior, and any microstructural model of white matter mechanics would require careful consideration of both the axon's tortuosity and the dynamics of kinematic coupling [18].

If heterogeneous, periaxonal cell-cell coupling is responsible for the transfer to affine kinematics, then we would expect injury to these cells to change with development as well. For instance, Mills et al. recently demonstrated that mechanical trauma to a mature, rat white matter preparation in vitro causes an initial wave of intracellular glial Ca2+ signal that spreads significantly from the location of trauma and can remain elevated in distal locations for over an hour [24]. A similar study in an immature white matter preparation could reveal different calcium dynamics because of alterations in axon-glia coupling and subsequent change in stress and strain distribution during trauma. Both primary and secondary injury to glia are critical components of the injury response that contribute significantly to the physiological and functional deficits observed post-trauma, and elucidating the underlying mechanisms of injury to these cells will represent a critical first step in understanding the evolution of secondary pathogenesis to healthy CNS tissue [24]. Moreover, it is possible that axons within specific regions of the spinal cord are more susceptible to traumatic injury due to the type (I/II versus III/IV) of oligodendrocytes and subsequent nature of glial coupling as well as the inherent tortuosity, and that the establishment of tortuosity and/or the nature of glial coupling represent evolutionary contributions to neuroprotection. A closer, tract-specific examination of axon kinematics with regard to oligodendrocyte phenotype, in combination with a model of white matter injury, is necessary to elucidate these relationships.

Lastly, we selected the developing chick embryo spinal cord as our model tissue, which confers several advantages for this study. Chick embryo tissue is readily available through procurement of fresh, fertilized eggs and is cost effective when compared to small mammals. Maintaining eggs during development is relatively simple, as is harvesting tissue at a desired developmental stage. The kinetics of spinal cord myelination in the chick have been well characterized [29,30,49], and myelination proceeds quickly, so it is easy to isolate spinal cords with different levels of myelination. Like the optic nerve, the spinal cord also provides a system in which the prevailing direction of axons is parallel to the direction of stretch, allowing a direct interpretation of the relationship between macroscopic tissue stretch and microscopic axonal deformation. Of course, the spinal cord is not purely white matter. Whereas gray matter will significantly contribute to the mechanostructural, material response (i.e., stress-strain response) of the spinal cord, we are largely interested in the kinematic coupling and pure strain-based behavior of white matter, which should be relatively independent of the gray matter. Comparing our results to the guinea pig optic nerve study, we found that the mean tortuosity of unstretched axons in the adult guinea pig optic nerve ($\sim$1.13) was greater than the tortuosity of chick embryo spinal cords at all stages ($\sim$1.096–1.083), and that the switching behavior in the optic nerve, as described by values of T_1 and T_2, was more coupled than the latest development stage examined [17]. Further, while we do not expect gray matter to significantly influence either initial tortuosity or white matter mechanics, the composition of the spinal cord and the optic nerve are markedly distinct. Chick embryo spinal cord and guinea pig optic nerve (or any

Downloaded From: https://biomechanical.asmedigitalcollection.asme.org on 04/23/2019 Terms of Use: http://www.asme.org/about-asme/terms-of-use

other white matter) axonal tortuosity and mechanics may follow the same functional form but require separate characterizations to capture the individual tortuosity and kinematics.

Acknowledgment

Funding for this study was provided by the Whitaker Foundation (RG 02-0128). We greatly appreciate the assistance of Alexander Kanevsky in tracing axons, and the assistance of Jeff Golda and John Hewitt in manufacturing the controlled stretch device.

References

[1] Kakulas, B. A., 1999, "A Review of the Neuropathology of Human Spinal Cord Injury With Emphasis on Special Features," J. Spinal Cord Med., **22**(2), pp. 119–124.
[2] Gentleman, S. M., Roberts, G. W., Gennarelli, T. A., Maxwell, W. L., Adams, J. H., Kerr, S., and Graham, D. I., 1995, "Axonal Injury: A Universal Consequence of Fatal Closed Head Injury?" Acta Neuropathol. (Berl), **89**(6), pp. 537–543.
[3] Graham, D. I., Adams, J. H., Nicoll, J. A., Maxwell, W. L., and Gennarelli, T. A., 1995, "The Nature, Distribution and Causes of Traumatic Brain Injury," Brain Pathol., **5**(4), pp. 397–406.
[4] Meaney, D. F., Margulies, S. S., and Smith, D. H., 2001, "Diffuse Axonal Injury," J. Neurosurg., **95**(6), pp. 1108–1110.
[5] Crowe, M. J., Bresnahan, J. C., Shuman, S. L., Masters, J. N., and Beattie, M. S., 1997, "Apoptosis and Delayed Degeneration After Spinal Cord Injury in Rats and Monkeys," Nat. Med., **3**(1), pp. 73–76.
[6] Grossman, S. D., Rosenberg, L. J., and Wrathall, J. R., 2001, "Temporal-Spatial Pattern of Acute Neuronal and Glial Loss After Spinal Cord Contusion," Exp. Neurol., **168**(2), pp. 273–282.
[7] Bain, A. C., Raghupathi, R., and Meaney, D. F., 2001, "Dynamic Stretch Correlates to Both Morphological Abnormalities and Electrophysiological Impairment in a Model of Traumatic Axonal Injury," J. Neurotrauma, **18**(5), pp. 499–511.
[8] Bain, A. C., and Meaney, D. F., 2000, "Tissue-Level Thresholds for Axonal Damage in an Experimental Model of Central Nervous System White Matter Injury," ASME J. Biomech. Eng., **122**(6), pp. 615–622.
[9] Maxwell, W. L., Islam, M. N., Graham, D. I., and Gennarelli, T. A., 1994, "A Qualitative and Quantitative Analysis of the Response of the Retinal Ganglion Cell Soma After Stretch Injury to the Adult Guinea-Pig Optic Nerve," J. Neurocytol., **23**(6), pp. 379–392.
[10] Gennarelli, T. A., Thibault, L. E., Tipperman, R., Tomei, G., Sergot, R., Brown, M., Maxwell, W. L., Graham, D. I., Adams, J. H., Irvine, A., Genarrelli, L. M., Duhaime, A. C., Boock, R., and Greenberg, J., 1989, "Axonal Injury in the Optic Nerve: A Model Simulating Diffuse Axonal Injury in the Brain," J. Neurosurg., **71**(2), pp. 244–253.
[11] Jafari, S. S., Maxwell, W. L., Neilson, M., and Graham, D. I., 1997, "Axonal Cytoskeletal Changes After Non-Disruptive Axonal Injury," J. Neurocytol., **26**(4), pp. 207–221.
[12] Jafari, S. S., Nielson, M., Graham, D. I., and Maxwell, W. L., 1998, "Axonal Cytoskeletal Changes After Nondisruptive Axonal Injury. II. Intermediate Sized Axons," J. Neurotrauma, **15**(11), pp. 955–966.
[13] Shi, R., and Pryor, J. D., 2002, "Pathological Changes of Isolated Spinal Cord Axons in Response to Mechanical Stretch," Neuroscience, **110**(4), pp. 765–777.
[14] Rosenberg, L. J., and Wrathall, J. R., 1997, "Quantitative Analysis of Acute Axonal Pathology in Experimental Spinal Cord Contusion," J. Neurotrauma, **14**(11), pp. 823–838.
[15] Blight, A. R., and Decrescito, V., 1986, "Morphometric Analysis of Experimental Spinal Cord Injury in the Cat: The Relation of Injury Intensity to Survival of Myelinated Axons," Neuroscience, **19**(1), pp. 321–341.
[16] Breig, A., 1960, *Biomechanics of the Central Nervous System*, Almqvist & Wiksell, Stockholm.
[17] Bain, A. C., Shreiber, D. I., and Meaney, D. F., 2003, "Modeling of Microstructural Kinematics During Simple Elongation of Central Nervous System Tissue," ASME J. Biomech. Eng., **125**(6), pp. 798–804.
[18] Meaney, D. F., 2003, "Relationship Between Structural Modeling and Hyperelastic Material Behavior: Application to CNS White Matter," Biomech. Model Mechanobiol., **1**(4), pp. 279–293.
[19] Charles, P., Tait, S., Faivre-Sarrailh, C., Barbin, G., Gunn-Moore, F., Denisenko-Nehrbass, N., Guennoc, A. M., Girault, J. A., Brophy, P. J., and Lubetzki, C., 2002, "Neurofascin is a Glial Receptor for the Paranodin/Caspr-Contactin Axonal Complex at the Axoglial Junction," Curr. Biol., **12**(3), pp. 217–220.
[20] Peles, E., Nativ, M., Lustig, M., Grumet, M., Schilling, J., Martinez, R., Plowman, G. D., and Schlessinger, J., 1997, "Identification of a Novel Contactin-Associated Transmembrane Receptor With Multiple Domains Implicated in Protein-Protein Interactions," EMBO J., **16**(5), pp. 978–988.
[21] Kakunaga, S., Ikeda, W., Itoh, S., Deguchi-Tawarada, M., Ohtsuka, T., Mizoguchi, A., and Takai, Y., 2005, "Nectin-like Molecule-1/TSLL1/SynCAM3: A Neural Tissue-Specific Immunoglobulin-like Cell-Cell Adhesion Molecule Localizing at Non-junctional Contact Sites of Presynaptic Nerve Terminals, Axons and Glia Cell Processes," J. Cell. Sci., **118**, pp. 1267–1277.
[22] Butt, A. M., Colquhoun, K., Tutton, M., and Berry, M., 1994, "Three-Dimensional Morphology of Astrocytes and Oligodendrocytes in the Intact Mouse Optic Nerve," J. Neurocytol., **23**(8), pp. 469–485.
[23] Casha, S., Yu, W. R., and Fehlings, M. G., 2001, "Oligodendroglial Apoptosis Occurs Along Degenerating Axons and is Associated With FAS and p75 Expression Following Spinal Cord Injury in the Rat," Neuroscience, **103**(1), pp. 203–218.
[24] Mills, L. R., Velumian, A. A., Agrawal, S. K., Theriault, E., and Fehlings, M. G., 2004, "Confocal Imaging of Changes in Glial Calcium Dynamics and Homeostasis After Mechanical Injury in Rat Spinal Cord White Matter," Neuroimage, **21**(3), pp. 1069–1082.
[25] Niebroj-Dobosz, I., Fidzianska, A., Rafalowska, J., and Sawicka, E., 1980, "Correlative Biochemical and Morphological Studies of Myelination in Human Ontogenesis. I. Myelination of the Spinal Cord," Acta Neuropathol. (Berl), **49**(2), pp. 145–152.
[26] Paus, T., Zijdenbos, A., Worsley, K., Collins, D. L., Blumenthal, J., Giedd, J. N., Rapoport, J. L., and Evans, A. C., 1999, "Structural Maturation of Neural Pathways in Children and Adolescents: In vivo Study," Science, **283**(5409), pp. 1908–1911.
[27] Nicolet, G., 1971, "Avian Gastrulation," Adv. Morphog, **9**, pp. 231–262.
[28] O'Donovan, M., Sernagor, E., Sholomenko, G., Ho, S., Antal, M., and Yee, W., 1992, "Development of Spinal Motor Networks in the Chick Embryo," J. Exp. Zool., **261**(3), pp. 261–273.
[29] Anderson, E. S., Bjartmar, C., and Hildebrand, C., 2000, "Myelination of Prospective Large Fibres in Chicken Ventral Funiculus," J. Neurocytol., **29**(10), pp. 755–764.
[30] Macklin, W. B., and Weill, C. L., 1985, "Appearance of Myelin Proteins During Development in the Chick Central Nervous System," Dev. Neurosci. (Basel, Switz.), **7**(3), pp. 170–178.
[31] Shrager, R., Jutan, A., and Muzik, R., 1994, LEASQ, GNU General Public License, Boston.
[32] Smith, D. H., Wolf, J. A., and Meaney, D. F., 2001, "A New Strategy to Produce Sustained Growth of Central Nervous System Axons: Continuous Mechanical Tension," Tissue Eng., **7**(2), pp. 131–139.
[33] Fass, J. N., and Odde, D. J., 2003, "Tensile Force-Dependent Neurite Elicitation via Anti-beta1 Integrin Antibody-Coated Magnetic Beads," Biophys. J., **85**(1), pp. 623–636.
[34] Heidemann, S. R., and Buxbaum, R. E., 1991, "Growth Cone Motility," Curr. Opin. Neurobiol., **1**(3), pp. 339–345.
[35] Bray, D., 1984, 'Axonal Growth in Response to Experimentally Applied Mechanical Tension," Dev. Biol., **102**(2), pp. 379–389.
[36] Abe, I., Ochiai, N., Ichimura, H., Tsujino, A., Sun, J., and Hara, Y., 2004, "Internodes Can Nearly Double in Length With Gradual Elongation of the Adult Rat Sciatic Nerve," J. Orthop. Res., **22**(3), pp. 571–577.
[37] Lindsey, J. K., Byrom, W. D., Wang, J., Jarvis, P., and Jones, B., 2000, "Generalized Nonlinear Models for Pharmacokinetic Data," Biometrics, **56**(1), pp. 81–88.
[38] Smith, D. H., Wolf, J. A., Lusardi, T. A., Lee, V. M., and Meaney, D. F., 1999, "High Tolerance and Delayed Elastic Response of Cultured Axons to Dynamic Stretch Injury," J. Neurosci., **19**(11), pp. 4263–4269.
[39] Mueller, H., Butt, H. J., and Bamberg, E., 1999, "Force Measurements on Myelin Basic Protein Adsorbed to Mica and Lipid Bilayer Surfaces Done With the Atomic Force Microscope," Biophys. J., **76**(2), pp. 1072–1079.
[40] Butt, A. M., Ibrahim, M., and Berry, M., 1998, "Axon-Myelin Sheath Relations of Oligodendrocyte Unit Phenotypes in the Adult Rat Anterior Medullary Velum," J. Neurocytol., **27**(4), pp. 259–269.
[41] Del Rio Hortega, P., 1922, "Son Homologables la Glia de Escasas Radiaciones y la Celula de Scwann," Bol. R. Soc. Esp. Hist. Nat., **10**, pp. 25–29.
[42] Del Rio Hortega, P., 1924, "La Glie a Radiations Peu Nombreuses et la Cellule de Schwann sont Elles Homologables," C R. Seances Soc. Biol. Fil, **91**, pp. 818–820.
[43] Hildebrand, C., Remahl, S., Persson, H., and Bjartmar, C., 1993, "Myelinated Nerve Fibres in the CNS," Prog. Neurobiol., **40**(3), pp. 319–384.
[44] Schwab, M. E., and Schnell, L., 1989, "Region-Specific Appearance of Myelin Constituents in the Developing Rat Spinal Cord," J. Neurocytol., **18**(2), pp. 161–169.
[45] Nolte, J., 1993, *The Human Brain: An Introduction to its Functional Anatomy*, 3rd ed., Mosby-Year Book, Inc., St. Louis.
[46] Gefen, A., Gefen, N., Zhu, Q., Raghupathi, R., and Margulies, S. S., 2003, "Age-Dependent Changes in Material Properties of the Brain and Braincase of the Rat," J. Neurotrauma, **20**(11), pp. 1163–1177.
[47] Prange, M. T., and Margulies, S. S., 2002, "Regional, Directional, and Age-Dependent Properties of the Brain Undergoing Large Deformation," ASME J. Biomech. Eng., **124**(2), pp. 244–252.
[48] Raghupathi, R., and Margulies, S. S., 2002, "Traumatic Axonal Injury After Closed Head Injury in the Neonatal Pig," J. Neurotrauma, **19**(7), pp. 843–853.
[49] State, F. A., El-Eishi, H. I., and Hamed, M. S., 1997, "Myelination and Cholinesterase Activity of Chick Embryo Spinal Cord," Acta Anat. (Basel), **99**(4), pp. 469–476.

Downloaded From: https://biomechanical.asmedigitalcollection.asme.org on 04/23/2019 Terms of Use: http://www.asme.org/about-asme/terms-of-use